1 **Cloud properties over the Southern Ocean during the MARCUS field**

2 **campaign**

3

4 Baike Xi[1], Xiquan Dong[1], Xiaojian Zheng[1], and Peng Wu[2]

5

6 [1]Department of Hydrology and Atmospheric Sciences, University of Arizona, Tucson, AZ, USA

7 [2]Pacific Northwest National Laboratory, Richland, WA, USA

8

9 **Correspondence:** Baike Xi (baikex@arizona.edu)

10

11 **Abstract.** To investigate the cloud properties over the Southern Ocean (SO), the MARCUS field

12 campaign (41 to 69 °S; 60 to 160 °E) was conducted from October 2017 to March 2018, using

13 ship-based measurements. To examine cloud properties over the mid-latitude and Polar regions,

14 the study domain is separated into northern (NSO) and southern (SSO) parts of the SO with a

15 demarcation line of 60 °S. The total cloud fractions (*CF*s) were 77.9 %, 67.6 %, and 90.3 % for

16 the entire domain, NSO and SSO, respectively, indicating that higher *CF*s were observed in the

17 Polar region. Low-level clouds, deep cumulus, and shallow cumulus clouds are the three most

18 common cloud types over the SO. For single-layered low-level clouds, mixed-phase clouds

19 dominate with an occurrence frequency (*Freq*) of 54.5 %, while the *Freq* of the liquid and ice

20 clouds were 10.1 % (most drizzling) and 17.4 % (least drizzling). The meridional distributions of

21 low-level cloud boundaries are nearly independent of latitude, whereas the cloud temperatures

22 increased ~ 8 K and atmospheric precipitable water vapor increased from ~5 mm at 69 °S to ~18

23 mm at 43 °S. The mean cloud liquid water paths over NSO were much larger than those over SSO.

24   Most liquid clouds occurred over NSO with very few over SSO, whereas more mixed-phase clouds

25   occurred over SSO than over NSO. There were no significant differences for ice cloud *Freq*

26   between NSO and SSO. These results will be valuable for advancing our understanding of the

27   meridional and vertical distributions of clouds and can be used to improve model simulations over

28   the SO.

29

30   **1. Introduction**

31   The Southern Ocean (SO) is one of the cloudiest and stormiest regions on the Earth (Chubb et

32   al., 2013). The majority of the aerosols are naturally produced via oceanic sources given the remote

33   environment. However, we have limited knowledge about cloud formation processes within such

34   clean environments and their associated aerosol and cloud properties. The unique nature of the SO

35   region features low-level supercooled liquid and mixed-phase clouds, which is significantly

36   different from the subtropical marine boundary layer (MBL) clouds where warm liquid clouds are

37   dominant (Dong et al., 2014; Wu et al., 2020; Zhao et al., 2020). Large biases in cloud amount and

38   microphysics over the SO in the Coupled Model Intercomparison Project phase 5 (CMIP5) climate

39   models result in a near 30 W m^{-2} shortwave radiation deficit at the top of the atmosphere (TOA)

40   (Marchand et al., 2014; Stanfield et al., 2014, 2015), which further leads to unrealistic cloud

41   feedbacks and equilibrium climate sensitivity (Bony et al., 2015; Stocker et al., 2013). Meanwhile,

42   the efficiency of aerosol-cloud interaction (ACI) over the SO was found to be crucial for the

43   models' sensitivities to the radiation budget. A new aerosol scheme in the Hadley Centre Global

44   Environmental model can dampen the ACI and suppress negative clear-sky shortwave feedback,

45   both of which contribute to a larger climate sensitivity (Bodas-Salcedo et a., 2019).

46   A climate sensitivity study using CMIP6 general circulation models (GCMs) shows much

47   higher temperature variations across 27 GCMs in response to doubled CO_2 than those in CMIP5,

48   which may have resulted from the decreased extratropical low-level cloud cover and cloud albedo

49   over the SO in CMIP6 (Zelinka et al., 2020). Low-level clouds are a key climate uncertainty and

50   can explain 50 % of the inter-model variations (Klein et al., 2017) because conversion from liquid

51   cloud droplets to ice cloud particles decreases the cloud albedo and reduces the reflected shortwave

52   radiation at TOA. Models, however, have difficulties accurately partitioning the cloud phase

53   (Kalesse et al., 2016). The phase changes in mixed-phase clouds over the Arctic have proved to

54   affect the cloud lifetime and radiative properties significantly, that is, converting from ice cloud

55   particles to liquid cloud droplets may increase the cloud optical depth and the reflected shortwave

56   radiation at TOA (Morrison et al., 2012). In contrast, models that allow mixed-phase clouds to

57   glaciate rapidly can produce 30% more warming from doubling CO_2 (McCoy et al., 2014).

58   Phase transition processes have been investigated by several groups using both satellite and

59   ground-based measurements. A study (Mace and Protat, 2018) found that there are more mixed-

60   phase clouds over the SO measured from the ship than retrieved from CloudSat and CALIPSO

61   measurements because the satellites cannot accurately measure clouds below ~1 km. A previous

62   study (Lang et al., 2018) used a model to investigate the clouds under post cold frontal systems

63   and found large biases in model simulations and concluded that the cloud cover and radiative

64   biases over the SO are highly regime dependent. Of all cloud types, low-level clouds are primarily

65   responsible for the biases in the model simulations due to the lack of reliable measurements, which

66   leads to a poor understanding of the conditions where these clouds form and the phase(s) that result.

67   In other words, a physical representation of clouds, especially for low-level clouds, is unclear but

68   truly necessary for improving model simulations. Therefore, reliable observations of the cloud

69   macro- and micro-physical properties from ground-based active and passive remote sensors are

70   crucial for the improvement of model simulations.

71   Previous studies show that cloud phase is primarily dependent on cloud temperature, and the

72   transition from one cloud phase to another will modify the cloud optical properties, which further

73   affects the radiation budgets (Hu et al., 2010; Intrieri et al., 2002; Morrison et al., 2012). Based on

74   satellite observations and retrievals, they found that supercooled liquid water (SLW) clouds are

75   most common in the low-level clouds over the SO, where 80% of low-level clouds contain SLW

76   in a wide range of cloud temperatures from 0°C to −40°C (Hu et al., 2010). The formation of SLW

77   clouds is usually related to strong boundary layer convection. However, when ice nuclei exist in

78   the mixed-phase clouds, the ice particles can grow quickly and become bigger through consuming

79   supercooled liquid water drops. The SLW is inherently unstable due to the higher vapor pressure

80   over liquid than over ice and the quicker vapor deposition on ice particles than on liquid droplets

81   (Intrieri et al., 2002). As the supercooled liquid cloud droplets glaciate to ice particles, the cloud

82   layer becomes darker because the ice particles scatter less shortwave radiation and absorb more

83   radiation in the near IR wavelength regime. It is unclear, however, what role these ice particles

84   play in the low-level clouds over the SO, which includes the impact on drizzle development.

85   During HIAPER Pole-to-Pole Observation (HIPPO) campaigns, the study in Chubb et al. (2013)

86   found that there are rarely ice particles in non-drizzling and light drizzling clouds over the SO,

87   which may imply that the ice particles in the mixed-phase clouds may modulate the drizzle

88   formation.

89   To investigate the aerosol and cloud properties over the SO, a field campaign called the

90   Measurements of Aerosols, Radiation, and Clouds over the Southern Ocean (MARCUS) was

91   conducted using the ship-based measurements between Hobart, Australia, and the Antarctic during

92   the period October 2017-March 2018. The Department of Energy (DOE) Atmospheric Radiation

93   Measurement (ARM) Mobile Facility (AMF2) was installed on the Australian icebreaker *Aurora*

94   *Australis,* which voyaged from Hobart, Tasmania to the Australian Antarctic stations of Casey,

95   Mawson, and Davis, as well as Macquarie Island as illustrated in Fig. 1. Another field campaign,

96   called South Ocean Clouds, Radiation, Aerosol Transport Experimental Study (SOCRATES) field

97   campaign was conducted during austral summer from January 15 to February 26, 2018, which in-

98   situ measurements may use as a reference for this analysis. The SOCRATES domain has shown

99   as black dotted rectangle box in Fig. 1. The objectives of the MARCUS campaign are to investigate

100   the vertical distribution of boundary layer clouds and reveal the reasons why the mixed-phase

101   clouds are common in the warm season (McFarquhar et al., 2016), which will be our focuses for

102   this study.

103   MARCUS ship-based instruments include AMF2 cloud radar, lidar, microwave radiometer,

104   micropulse lidar, radiosonde sounding, precision solar pyranometer and precision infrared

105   radiometer, as well as aerosol sensors. Through these comprehensive observations over the SO,

106   we are tentatively answering the following three scientific questions:

107   (1)   What is the total cloud fraction over the SO during MARCUS, as well as vertical

108   and meridional variations in cloud fraction?

109   (2)   What are the dominant cloud types over the SO, their associated cloud properties,

110   as well as their vertical and meridional distributions?

111   (3)   What are the vertical and meridional distributions of the low-level clouds over the

112   SO?

113   This manuscript is organized as follows: the data and method are introduced in section 2. The

114   statistical results for all clouds during MARCUS are summarized in section 3. The low-level cloud

115   properties are described in section 4, followed by a summary and conclusions in section 5.

116

117   **2. Data and Method**

118   The cloud properties analyzed in this study are derived from the data collected by AMF2,

119   including the 95-GHz W-band cloud radar, ceilometer, micropulse lidar, microwave radiometer,

120   aerosol observation system (AOS), meteorological measurements (MET, includes the following

121   data: temperature, pressure, specific humidity, wind direction, and speed) on the ship, rain gauge

122   and the radiosonde soundings. The combined cloud radar and ceilometer measurements can

123   provide the cloud boundaries as long as there are no optically thin clouds and the cloud-base

124   heights (H_{base}) are not greater than the upper limit (7.7 km) of the ceilometer. The micropulse lidar

125   will be used to identify optically thin clouds and the clouds with $H_{base} > 7.7$ km. A previous study

126   has shown that these additional clouds detected by the micropulse lidar can be a non-negligible

127   supplement to the total cloud fraction (Mace et al., 2021). There are about 4 to 5 radiosonde

128   soundings per day. We adopted a linear interpolation method based on these daily soundings to

129   achieve a better temporal resolution of temperature, pressure, and specific humidity. The method

130   considers MET measurements to ensure vertical continuity and adjacent soundings for temporal

131   continuity. Using these interpolated atmospheric profiles, cloud temperatures can be accurately

132   estimated.

133   The cloud occurrence frequency can be determined through two steps: the column cloud

134   fraction is simply the ratio of cloudy samples to the total observations in every 5-min; the

135   occurrence frequency for each type of cloud during the entire time period equals the ratio of the

136   number where column cloud fraction is greater than zero to the total 5-min samples. The cloud

137   liquid water path (*LWP*) and atmospheric precipitable water vapor (*PWV*) are retrieved based on a

138   physical-iterative algorithm using observations of the microwave radiometer brightness

139   temperature at 23.8 and 31.4 GHz with uncertainties ranging from 15 to 30 g m^{-2} (Marchand et al.,

140   2003). It is important to note that the brightness temperature biases switch signs among different

141   climatological regions because a threshold of 5 ℃ in cloud-base temperature was used in their

142   physical retrievals. Therefore, we propose an extra step to determine the uncertainties during

143   MARCUS. Both the AOS and rain gauge measurements were used to determine whether rain is

144   reaching the surface qualitatively, but not quantitatively in this study. All the measurements were

145   averaged over 5 minutes except radar reflectivity, Doppler velocity, and spectrum width used in

146   Section 4.3. The detailed classification method will be introduced in Section 4.1. In brief, we used

147   the measurements of interpolated sounding, microwave radiometer retrieved *LWP*, radar

148   reflectivity, Doppler velocity and spectrum width to classify the cloud phase in each radar range

149   volume of low-level clouds during MARCUS. We also used ERA5 reanalysis data to study the

150   environmental conditions during MARCUS and calculated the lower tropospheric stability (LTS)

151   and estimated inversion strength (EIS) when the low-level clouds appeared along the shiptracks.

152   A classification method developed in Xi et al. (2010) was used to calculate the occurrence

153   frequencies of different types of clouds and their corresponding cloud macrophysical properties,

154   e.g., cloud base (H_{base}) and top (H_{top}) heights, cloud thickness (ΔH), and *LWP*. The relative

155   contributions of mixed-phase, liquid and ice clouds to the single-layered low-level clouds as well

156   as their drizzling status are analyzed in this study. To further investigate the drizzling status under

157   different cloud phases, we also calculated their LTS and EIS. The latitudinal and longitudinal

Atmospheric
Measurement
Techniques
Discussions
Open Access
EGU

158   variations of the single-layered low-level clouds as well as their vertical distributions are also

159   explored in this study.

160

161   **3. Statistical results for all clouds during MARCUS**

162   The occurrence frequencies of total cloud cover and different types of clouds and their

163   associated properties over the entire study domain during MARCUS are presented in Figs. 2-4. In

164   order to examine the cloud properties over the mid-latitude and Polar regions, we separate the SO

165   domain into northern (NSO, north of 60°S) and southern (SSO, south of 60°S) parts using a

166   demarcation line of 60°S. A total of 2,447 hours cloud samples were collected during MARCUS

167   in this study, in which 1,181 hours of samples were located in the NSO and 1,266 hours of samples

168   were collected from the SSO. It is important to note that adding micropulse lidar measurements

169   increased the total samples of non-liquid-containing clouds by ~20% because micropulse lidar is

170   more sensitive to optically thin clouds than cloud radar. However, micropulse lidar signals are

171   usually attenuated and cannot provide a meaningful signal when the liquid cloud layer is thicker

172   than a couple of hundred meters (Sassen, 1991).

173   Figure 2 shows the vertical distributions of total cloud cover over the entire domain, as well as

174   over NSO and SSO. For the vertical distributions, the occurrence frequencies of total cloud

175   increase from the first radar gate (~ 226 m) to ~700 m, then monotonically decrease with altitude

176   with a few small increments at different levels, especially over SSO. We can draw the following

177   conclusions by comparing the occurrence frequencies of the total cloud between NSO and SSO. 1)

178   The SSO has more cloudiness than the NSO under 7 km, while the NSO has more cloudiness than

179   the SSO above 7 km. 2) Below 3 km, the occurrence frequencies of clouds over the NSO decrease

180   dramatically from 37 % at an altitude of ~700 m to 16 % at 3 km and from 45 % to 28 % over the

Atmospheric
Measurement
Techniques

Discussions

EGU

Open Access

181 SSO, which is similar to the vertical distributions of the low-level clouds over some Northern

182 Hemisphere mid-latitude regions, such as Eastern North Atlantic (ENA, Dong et al., 2014). The

183 occurrence frequencies measured during MARCUS are much lower than these shown in Fig. 8 of

184 Mace et al. (2009) throughout the entire vertical column between the same range of latitudes,

185 especially, the occurrence frequencies during MARCUS are almost half of these measured by

186 CloudSat and CALIPSO from 1 to 3 km. The reason has been explained in Xi et al. (2010), that is,

187 a comparison of occurrence frequencies between measurements of two different platforms can

188 only be performed under an equivalent spatial-to-temporal resolution. In other words, our results

189 were calculated under 5-min temporal resolution, and the results in Mace et al. (2009) were

190 statistically in the 2 ° grid box. Therefore, the comparison between these two results is not

191 reasonable. To make a fair comparison, one has to know the cloud amount at each area or time

192 step, then the product of amount and frequency is independent of either temporal and spatial

193 measurement.

194 To compare with other studies, we calculated the cloud fractions (*CF*s) of total and different

195 types of clouds. The total *CF*s were 77.9 %, 67.6 %, and 90.3 % for the entire domain, NSO and

196 SSO, respectively, indicating that 22.7 % more clouds occurred in the Polar region than in the mid-

197 latitude region. The total *CF* over the entire domain is very close to the 76 % calculated by Mace

198 and Protat (2018) using ship-based measurements during the Cloud, Aerosols, Precipitation,

199 Radiation and Atmospheric Composition (CAPRICORN) field experiment. The total *CF* over the

200 SSO is very close to that estimated by using the complementarity of CALIOP lidar aboard

201 CALIPSO and CPR aboard CloudSat (DARDAR version 2 data) from Listowski et al. (2019).

202 Figure 3 shows the occurrence frequencies of categorized clouds and their cloud boundaries

203 using the maximum H_{top} and the minimum H_{base}. The definition of each type of cloud follows the

Atmospheric
Measurement
Techniques
Discussions

Open Access

EGU

204   method of Xi et al. (2010). A brief description of the classification of cloud types is as follows.

205   The single-layered low-level clouds (LOW) is the fraction of time when low clouds with $H_{top} \leq 3$

206   km occur without clouds above them. Middle clouds (MID) range from 3 to 6 km without any

207   clouds below and above, while high clouds (HGH) have $H_{base} > 6$ km with no cloud underneath.

208   Other types of clouds are defined by different combinations of the above three types, middle over

209   low (MOL), high over low (HOL), high over mid (HOM), and the cloud column through the entire

210   troposphere is defined as HML. Three types, MOL, HOM, and HML, include both contiguous and

211   non-contiguous cloud layers, and their thicknesses may be overestimated when clear layer(s) are

212   present between any two cloud layers.

213   As illustrated in Fig. 3a, the single-layered low-level (LOW), deep cumulus or multi-layered

214   (HML), and shallow cumulus (MOL) clouds are the three dominant types of clouds over the SO.

215   Comparing the clouds between NSO and SSO, all types of clouds in SSO are higher than those in

216   NSO except HOL. The differences range from less than 1 % (LOW) to more than 10 % (MOL).

217   Comparing the clouds over mid-latitude oceans between the two hemispheres, i.e., between NSO

218   and ARM ENA site (Dong et al., 2014), we find: (1) The total cloud fractions (CFs) are close to

219   each other (67.6 % over NSO vs. 70.1 % at ARM ENA); (2) LOW CFs are 22.9 % vs. 27.1 %,

220   which is the dominant type of cloud in both regions; and (3) Both MOL and HML clouds, including

221   underneath low clouds, are 14.2 % and 16.5 % over NSO, much higher than those (4.2 % and

222   12.1 %) at ARM ENA site, indicating that there are more shallow and deep convective clouds over

223   NSO than over ENA.

224   Figure 3b shows the vertical locations of different types of cloud layers, which represent the

225   maximum H_{top} and minimum H_{base}, as well as their deepest ΔH for any type of cloud. Nearly all

226   H_{top} and ΔH values over NSO are higher or deeper than those over SSO, presumably due to stronger

227   solar radiation and stronger convection over NSO. H_{base} values basically followed their cloud-top

228   counterparts with a couple of exceptions. These cloud properties are closely associated with large-

229   scale dynamic patterns and environmental conditions. By analyzing the ERA-I reanalysis (not

230   shown), the 850 hPa geopotential heights show persistent westerlies with slightly higher

231   geopotential heights over the northwest corner of the domain, which may closely relate to the

232   higher H_{top} over NSO than over SSO. Furthermore, the boundary layer over NSO is relatively more

233   stable than over SSO based on lower troposphere stability analysis.

234   When we plot the probability density functions (PDFs) of cloud LWPs for different types of

235   clouds, we find that the PDFs of LWPs for HGH and HOM peak at less than 10 g m^{-2}. These results

236   make physical sense because HGH clouds should not contain any liquid droplets, and most HOM

237   clouds, especially those over SSO, should be ice phase dominant. In addition, the 10 g m^{-2} of LWP

238   is close to the uncertainty of the LWP retrieval in Marchand et al. (2003). Therefore, this value is

239   used as a threshold for all types of clouds, which leads to less than one percent reduction of the

240   total samples. As shown in Fig. 4a, the LWPs ($>$ 10 g m^{-2}) for all types of clouds are much higher

241   over NSO than over SSO because the low-level and shallow convective clouds in the mid-latitudes

242   contain more liquid water than those in Polar regions. The mean LWPs for liquid containing low-

243   level and middle-level clouds over NSO, such as LOW, MID and HOL, range from ~130 to 150 g

244   m^{-2}, while the mean LWPs for shallow and deep convective clouds, such as MOL and HML, are

245   two times higher (~270 g m^{-2}) than the mean LWP of LOW, MID and HOL. Note that the mean

246   LWPs for most types of clouds over the SSO are much lower than those over the NSO, except for

247   the LOW clouds.

248   Table 1 provides a summary of the average, standard derivation, minimum and maximum for

249   cloud boundaries, liquid water path and the percentage of multi-layered cloud for each cloud type

250   over the SO. Non-contiguous clouds over the SO occur very frequently, especially for HOM and

251   HML. The *LWP* for single-layered clouds is greater than that for multi-layered clouds. The *LWP*

252   for single-layered HML almost doubles that for multi-layered HML.

253   The occurrence frequencies of *LWP*s (> 10 g m^{-2}) over NSO and SSO contradict their cloud

254   *LWP* counterparts, as demonstrated in Fig. 4b. To further investigate the amount of available

255   precipitable water vapor (*PWV*), we found that mean *PWV* values in SSO are at least 2 to 3 times

256   less than those in NSO for the same types of clouds (figure not shown). Note that the samples of

257   MID, HGH, and HOM clouds are excluded from this study when they have *LWP*s less than 10 g

258   m^{-2}, since these low *LWP*s are within the retrieval uncertainty of cloud *LWP* and hence may not

259   contain any liquid cloud droplets. The higher *LWP*s, larger cloud droplets, drizzle drops and ice

260   particles, and greater drizzling occurrence frequencies over NSO (which is discussed later) will

261   lead to the quick dissipation of clouds over NSO. In contrast to NSO, the SSO cloud *LWP*s and

262   particle sizes are much smaller with fewer drizzling events, which increases cloud lifetime relative

263   to NSO. The 67.6 % and 90.3 % *CF*s over NSO and SSO provide strong evidence for this argument.

264   We can draw the following conclusions by comparing the cloud properties between NSO and SSO

265   in Figs. 3 and 4. The LOW fraction, thickness, and *LWP* over NSO and SSO are comparable to

266   each other. For other types of clouds, cloud thicknesses are similar to each other or slightly deeper

267   over NSO, but the cloud *LWP*s over NSO are much larger than those over SSO, resulting in more

268   precipitation events over NSO. As pointed out in (Albrecht 1989), more precipitation events may

269   reduce the cloud lifetime. This argument is consistent with the results shown in Figs. 2 and 3a for

270   all clouds except for HOL. Cloud lifetimes over NSO are shorter than those over SSO, which leads

271   to lower *CF*s over NSO than over SSO.

272

Atmospheric
Measurement
Techniques
Discussions

Open Access

EGU

273   **4.   Single-layered low-level clouds**

274   As discussed in Section 3, single-layered low-level clouds (LOW) are the dominant cloud type

275   in both northern (NSO) and southern (SSO) parts of the SO. Figs. 3 and 4 further reveal that LOW

276   cloud type is the only one having comparable *CF*, cloud, thickness, *LWP* over both NSO and SSO.

277   This warrants further study: Are the cloud phases, properties, and vertical and meridional

278   variations of LOW clouds over these two regions similar to each other or significantly different?

279   **4.1. Cloud phase**

280   In this study, cloud boundaries are determined by combining cloud radar, ceilometer and

281   micropulse lidar measurements at a temporal resolution of 5-min. The cloud phase, liquid water

282   droplets or ice particles, are determined in each radar range volume. A flow chart for classifying

283   the phases of single-layered low-level clouds is drawn in Fig. 5. The determination of warm liquid

284   clouds is straightforward using both cloud-base (T_{base}) and -top (T_{top}) temperatures greater than 0

285   °C, and cloud *LWP*s greater than the threshold ($10\ \text{g m}^{-2}$). The determination of supercooled liquid

286   clouds is slightly complicated. When either T_{base} or T_{top} is below 0° C, and cloud *LWP*s are greater

287   than the threshold, the radar Doppler spectrum width (*WID*) and velocity (V_{d}) are used for the

288   determination of supercooled liquid water clouds. If the majority (10 seconds of original radar

289   measurements) of *WID* are less than $0.4\ \text{m s}^{-1}$ and V_{d} are equal to or less than $0.0\ \text{m s}^{-1}$ (updrafts)

290   in the volume, then this range volume is defined as supercooled liquid clouds.

291   Mixed-phase clouds are determined when the medians (calculated from 10 seconds of original

292   radar measurements) of *WID* is greater than $0.4\ \text{m s}^{-1}$ and V_{d} is greater than $0.0\ \text{m s}^{-1}$ (downdrafts)

293   due to the existence of large ice particles in the clouds. If cloud *LWP* is below the threshold, then

294   it is defined as an ice cloud, otherwise, it is defined as a mixed-phase cloud. It is worth mentioning

295   that large ice particles, which grow through vapor deposition or rime processes, dominate the radar

Atmospheric
Measurement
Techniques
Discussions

296   reflectivity and are heavier than cloud droplets. Therefore, these large ice particles not only

297   broaden the spectrum width but also have relatively large fall speeds.

298   To further evaluate our classification method, we compared the classified mixed-phase and ice

299   clouds with the micropulse lidar linear depolarization ratios (*LDR*) as an extra measure. The *LDR*

300   ranges follow the method in Shupe et al. (2005), which are $0.11 < LDR < 0.15$ for mixed-phase

301   clouds, and $LDR > 0.15$ for ice clouds. Table 2a shows the quantitative comparison of the cloud

302   phase identifications between these two classification methods. The numbers represent the counts

303   of each matched 5-min sample, where the diagonal numbers indicate that both methods are

304   identifying the same type of cloud phase. In general, the two methods have 89 % agreement on the

305   phase identification. Secondly, we performed the phase classification directly from microphysical

306   probes onboard G-1 aircraft during SOCRATES and treated them as 'ground-truth' (Mohrmann et

307   al., 2021). By changing the time step of sampling to mimic what the radar may observe the cloud

308   for each range volume, Table 2b shows the statistics of the possibility of the cloud phase that may

309   be detected by cloud radar. As sampling time increases from 1 second to 30 seconds, more mixed-

310   phase clouds and fewer single-phase clouds can be observed.

311   Figure 6 shows the occurrence frequencies of the matched results for mixed-phase clouds (left

312   panel) and ice clouds (right column). For the classified ice clouds, most of the Doppler spectrum

313   widths range from 0.08 to 0.16 m s^{-1} and the *LDR* ratios can be up to ~0.5, representing a narrow

314   range of ice particle size distribution with higher *LDR* ratios. Cloud liquid is identified by low *LDR*

315   of ~0.11 (Fig. 6d) and high lidar backscatter from 10^{-5} to 10^{-4} m^{-1} sr^{-1} (Fig. 6e). For the classified

316   mixed-phase clouds, most of the Doppler spectrum width range from 0.15 to 0.35 m s^{-1} and most

317   of the *LDR* signals are less than 0.4, representing a broad particle size distribution resulting from

318   the mixture of liquid droplets and ice particles but lower *LDR* ratios. Based on the Doppler velocity,

Atmospheric
Measurement
Techniques
Discussions

Open Access

EGU

319   the mode values for both mixed-phase and ice clouds occur at ~ 0.5 m s^{-1}, where the ice particles

320   are dominant in both types of clouds. The broader particle size distribution with lower *LDR* ratios

321   for mixed-phase clouds and narrower particle size distribution with higher *LDR* ratios for ice

322   clouds further corroborate that the classified results from this study are consistent with the

323   traditional micropulse lidar *LDR* method.

324   It is important to note that the micropulse lidar signals are usually attenuated and cannot

325   provide a meaningful signal when the liquid cloud layer is thicker than a couple of hundred meters

326   (Sassen, 1991). Arctic mixed-phase clouds are typical, with the liquid-dominant layer on the top

327   of the mixed-phase clouds and the ice-dominant layer underneath. The ceilometer-derived cloud-

328   base height represents the base of the liquid-dominant layer near the cloud top, while MPL-derived

329   cloud-base height represents the base of the lower ice-dominant layer (Qiu et al., 2015; Shupe,

330   2007; Shupe et al., 2005). Over the Arctic, the micropulse lidar signals can penetrate through the

331   ice-dominant layer to the liquid-dominant layer. However, the mixed-phase clouds over the

332   Southern Ocean are totally different from those over the Arctic region: they are well mixed (liquid

333   droplets and ice particles) from cloud base to cloud top, which is found in this study. Thus, the

334   micropulse lidar signals can be attenuated in the mixed-phase clouds over the Southern Ocean.

335   Statistical results show that 43 % of micropulse data were attenuated during MARCUS compared

336   to our classified results.

337   This classification method is further supported by the onboard cloud radar measurements

338   during the Southern Ocean Clouds Radiation Aerosol Transport Experimental Study (SOCRATES,

339   not shown). In that campaign, the reflectivity measurements were usually greater, and the spectrum

340   widths were much wider when the aircraft observed large ice particles compared to the time

341   periods when liquid cloud droplets were observed. It is also worth mentioning that about 5.5 % of

342   single-layered low-level cloud phases cannot be determined when the radar measurements were

343   not available during MARCUS. Therefore, using our classification method, a total of 6,934 5-min

344   single-layered low-level cloud samples were determined in this study, including 697 liquid cloud

345   samples, 3,777 mixed, 1,205 ice, and 1,255 'OTHER' clouds. The category of 'OTHER' clouds

346   represents more than one phase in each column.

347   Figure 7 (upper panel) shows the drizzling status for each categorized cloud type, e.g., no rain

348   (yellow-green), virga (brown) and rain (navy blue). The definition of drizzling status follows the

349   method in Wu et al., (2015, 2017), which used both ceilometer and cloud radar measurements to

350   determine the status of MBL clouds under non-drizzling, virga and rain conditions. The

351   percentages shown below the x-axis represent the portion of drizzling status in each type of clouds,

352   such as liquid, mixed-phase, ice and 'OTHER' clouds. Figure 7 (bottom panel) also shows the

353   percentages and vertical distributions of classified liquid, mixed-phase, ice, and 'OTHER' clouds

354   for each column in the single-layered low-level clouds, represented by different colors. After

355   classification, the samples in each category are sorted by their H_{top}. In detail, Fig. 7 demonstrates

356   that the mixed-phase clouds dominate the single-layered low-level cloud category with an

357   occurrence frequency of 54.5 %. The 'OTHER' and ice clouds have similar occurrence frequencies

358   of 18.1 % and 17.4 %, respectively, while the liquid clouds have the least occurrence frequency of

359   10.1 %. The liquid topped mixed-phase clouds (included in 'OTHER'), which frequently occur in

360   the Arctic region (Qiu et al., 2015), are rarely found over the SO. The existence of ice particles in

361   mixed-phase clouds should strongly depend on the distribution of ice nuclei (IN), whereas spatially

362   unevenly distributed IN may result in the OTHER type of clouds.

363   Based on the results in Fig. 7, we draw the following conclusions. Most of the ice clouds are

364   non-drizzling clouds, and the percentages with virga and drizzle below the cloud base are 12 %

365   and 15 %, respectively. The percentages of non-drizzling, virga and drizzling mixed-phase clouds

366   are 50 %, 21 %, and 29 %. The liquid and 'OTHER' clouds have similar percentages, they are 36 %,

367   25 % and 39 % for liquid clouds, and 35 %, 22 % and 44 % for 'OTHER' clouds. For liquid and

368   'OTHER' clouds, the drizzling frequencies are independent of H_{top}. In contrast, for mixed-phase

369   and ice clouds, the drizzling frequencies strongly depend on $H_{top,}$ i.e., higher drizzling frequencies

370   occur mostly at higher H_{top}.

371   The properties of single-layered low-level clouds are summarized in Table 3. The liquid clouds

372   have the lowest H_{base} and H_{top} but more available water vapor than other types of clouds. Since the

373   'OTHER' clouds are a transitional stage among mixed-phase, liquid and ice clouds, they have the

374   highest H_{top}, deepest cloud layer and largest LWP. The ice clouds occur in relatively dry

375   environments and have the highest H_{base} at 1.218 km. The mixed-phase clouds have similar H_{base},

376   but lower H_{top}, LWP and PWV compared to those of 'OTHER' clouds. Since LWPs in mixed-phase

377   clouds have larger standard deviations, which implies that SLW is more common at higher LWPs

378   and ice is more common at lower LWPs.

379   **4.2. Meridional variations of cloud properties**

380   Figure 8 shows the meridional variation in single-layered low-level cloud properties during

381   MARCUS. As illustrated in Fig. 8a, the meridional distributions of H_{base}, H_{top} and ΔH are nearly

382   independent of latitude, however, their corresponding temperatures (T_{base} and T_{top}) increased about

383   8 K from 69 $^{\circ}$S to 43 $^{\circ}$S, though there were slight fluctuations. These results suggest that the cloud

384   and sea surface temperatures have minimal impact on the cloud boundaries over the SO, which is

385   consistent with the findings in McFarquhar et al. (2016). The meridional variation of LWPs mimics

386   those of T_{base} and T_{top}, with an increasing trend from south to north. It is important to point out that

387   a big drop in LWP at ~50 °S results from fewer occurrences of low-level clouds there, indicating

388   that the cloud samples at some latitudes are not statistically significant. The atmospheric *PWV*

389   increased dramatically from ~ 5 mm at 69 $^\circ$S to ~18 mm at 43 $^\circ$S, presumably due to increased sea

390   surface and atmospheric temperatures.

391   Figure 9 shows the latitudinal and meridional distributions of categorized liquid, mixed-phase,

392   ice and 'OTHER' in single-layered low-level clouds over the SO during MARCUS. Each circle

393   represents the exact location and time along the ship track. Mixed-phase clouds occurred

394   everywhere over the SO during the MARCUS field campaign and became dominant in November,

395   December and February. Liquid clouds dominated in March, while ice clouds dominated in

396   January. The 'OTHER' clouds are a kind of transitional phase falling in between the mixed-phase

397   and ice/liquid clouds because there are no stand-alone occurrences in any month during MARCUS.

398   **4.3 Vertical distribution of cloud properties**

399   The vertical distributions of classified liquid, mixed-phase, and ice clouds are presented in Figs.

400   10-12. The focus of this section will be comparisons of cloud properties between the north (NSO)

401   and south (SSO) regions of the domain. Figure 10a shows the vertical distributions of liquid clouds,

402   which were capped at ~ 1.6 km, mostly in the marine boundary layer. The vertical occurrence

403   frequencies are up to 27 % over NSO, while they were less than 4 % over SSO, i.e., liquid clouds

404   occurred fairly often over the mid-latitude region, but very few occurred over the Polar region. On

405   the contrary, the occurrence frequencies of mixed-phase clouds between NSO and SSO are

406   opposite to liquid clouds, as illustrated in Fig. 10b, though the differences are not so obvious.

407   Mixed-phase clouds increased with altitude until ~1.6 km, then decreased monotonically towards

408   3 km. The highest frequencies were ~37 % at 0.6 km over SSO and ~27 % at 1.5 km over NSO.

409   The vertical distributions of ice clouds are similar to those of mixed-phase clouds (Fig. 10c).

410   However, there were no significant differences between NSO and SSO. It is worth mentioning that

411   the vertical distributions of mixed-phased clouds over SO are quite different to those from DOE

412   ARM Northern Slope Alaska (NSA) site where the liquid topped mixed-phase low-level clouds

413   are common (e.g., Qiu et al., 2015).

414   To further investigate the vertical distributions of classified liquid, mixed-phase, and ice clouds

415   over NSO and SSO, we plot the normalized vertical distributions (cloud base as 0, cloud top as 1)

416   of radar reflectivity, Doppler velocity and spectrum width in Figs. 11 and 12, respectively. In this

417   study, the threshold of -50 dBZ was used to determine the cloud boundary over the SO instead of

418   the threshold of -40 dBZ radar reflectivity used at the ARM ENA site (Dong et al., 2014). If we

419   used the threshold of -40 dBZ over the SO, then there would be only 73 % cloud samples available

420   for this study. About 9.6 % of radar reflectivities during MARCUS are less than -50 dBz for all

421   single-layered low-level cloud samples. Thus all radar parameters used in this study are based on

422   90.4 % of the radar measurements with reflectivity greater than -50 dBz.

423   Figures 11a-11c represent the normalized vertical distributions of radar reflectivity, Doppler

424   velocity and spectrum width of liquid clouds. Liquid clouds had the lowest reflectivity near the

425   cloud top because of cloud-top entrainment., The reflectivity had a nearly constant median value

426   of ~ -22 dBZ from near cloud top height (~ 0.8 for normalized height) of the cloud layer to the

427   cloud base. Most of the reflectivities were less than -15 dBz, which is the threshold to distinguish

428   cloud and drizzle-sized particles in each radar range volume (Wu et al., 2020). Most of the Doppler

429   velocities were greater than 0.0 m s^{-1}, indicating that downwelling motion is dominant in liquid

430   clouds. The profiles of Doppler velocity and spectrum width increased smoothly from the cloud

431   top to base, suggesting that larger cloud droplets and broader size distributions exist near the cloud

432   base, which is attributable to more drizzle drops near the cloud base, as illustrated in Fig. 7.

Atmospheric
Measurement
Techniques
Discussions

Open Access

EGU

433   The vertical distributions of mixed-phase clouds in Figs. 11d-11f are similar to those of liquid

434   clouds. The more occurrences of larger reflectivity measurements and larger median values of

435   spectrum width near the cloud base are most likely due to the presence of moderate ice particles

436   and/or drizzle drops. The nearly same median values of reflectivity, Doppler velocity and spectrum

437   width (but slightly larger standard deviations in each level in mixed-phase clouds) in both liquid

438   and mixed-phase clouds suggest that the ice particle sizes in mixed-phase clouds are comparable

439   to cloud droplets and drizzle drops. The nearly uniform vertical distributions of Doppler velocity

440   and spectrum width indicate well-mixed liquid cloud droplets and ice particles throughout the

441   cloud layer in the mixed-phase clouds over NSO.

442   Ice clouds had much lower reflectivity and narrower spectrum width than liquid and mixed-

443   phase clouds, as shown in Figs. 11g-11i. Almost all reflectivity measurements were less than -25

444   dBz with a median value of -35 dBz at the cloud base, resulting from small or moderate ice

445   particles but much lower concentration. A nearly constant Doppler velocity within the cloud layer

446   further supports the discussion of mixed-phase clouds above, i.e., the ice particle sizes are

447   independent of cloud height and comparable to liquid cloud droplets in the low-level clouds over

448   the SO. Because there are no mechanisms for growing large ice particles in such shallow ice clouds,

449   the accretion process cannot take place. From the statistical results in Fig. 7, these ice particles

450   have relatively little chance to become virga or raindrops and usually dissipate or transition to

451   other types of clouds.

452   Since there are not enough liquid cloud samples over the Polar region, only the mixed-phase

453   and ice clouds results are plotted in Fig. 12. Compared to the vertical distributions of ice clouds

454   over NSO, the median values of reflectivity and Doppler spectrum width over SSO were lower

455   and narrower, indicating a lack of large ice particles in the Polar region. The small ice particles in

456   the Polar region were also reflected in their mixed-phase clouds. Compared to the vertical

457   distributions of the mixed-phased clouds over NSO, the median values of reflectivity and Doppler

458   spectrum width over SSO were dramatically lower (-35 dBz at SSO vs. -22 dBz at NSO; 0.25 m

459   s^{-1} at SSO vs. 0.32 m s^{-1} at NSO). Figure 12 illustrates that the ice particle sizes over SSO are

460   smaller, their size distributions are narrower than those over NSO, indicating of lack of large ice

461   particles over SSO.

462

463   **5. Summary and Conclusions**

464   In this study, we presented the statistical results of clouds over the Southern Ocean (SO) and

465   the northern (NSO) and southern (SSO) parts during MARCUS IOP. We used the method

466   developed in Xi et al. (2010) to calculate the occurrence frequencies of different types of clouds

467   and their corresponding cloud macrophysical properties. We developed a new method to classify

468   liquid, mixed-phased, and ice clouds in the single-layered low-level clouds as well as their

469   corresponding drizzling status. Lastly, we explored the meridional and vertical distributions of

470   these classified cloud properties. Analysis of the MARCUS cloud properties has yielded the

471   following conclusions.

472   1.   The total cloud fractions (*CF*s) were 77.9 %, 67.6 %, and 90.3 % for the entire

473   domain, NSO and SSO, respectively, indicating that 22.7 % more clouds occurred in the Polar

474   region than in the mid-latitude region. The SSO had more clouds under 7 km, while the NSO

475   had more clouds above 7 km. Below 3 km, the occurrence frequencies of clouds over NSO

476   decrease dramatically from 37 % at an altitude of ~700 m to 16 % at 3 km, which is similar to

477   the vertical distributions of the low-level clouds over some Northern Hemisphere mid-latitude

478   regions, such as Eastern North Atlantic.

479   2.   The single-layered low-level (LOW), deep cumulus or multi-layered (HML), and

480   shallow cumulus (MOL) clouds are the three dominant types of clouds over the SO. Comparing

481   the clouds between NSO and SSO, all types of clouds in SSO are higher than those in NSO

482   except HOL. The LOW fraction, thickness, LWP over both NSO and SSO are comparable to

483   each other. The mean LWPs for low clouds over NSO, such as LOW, MOL and HOL, range

484   from ~130 to 150 g m^{-2}, while the mean LWPs for shallow and deep convective clouds, such

485   as MOL and HML, are two times (~270 g m^{-2}) higher than the same types of clouds. The mean

486   LWPs of clouds over SSO are much lower than the LWPs over NSO. Over the Southern Ocean,

487   the single-layered or contiguous clouds usually have higher liquid water paths than their

488   counterpart of multi-layered or non-contiguous clouds. There are more non-contiguous HML

489   and HOM than contiguous ones.

490   3.   A new method was developed to classify liquid, mixed-phase and ice clouds in the

491   single-layered low-level clouds (LOW) based on comprehensive ground-based observations.

492   The mixed-phase clouds are dominant in the single-layered low-level cloud category with an

493   occurrence frequency of 54.5 %. The 'OTHER' and ice clouds had similar occurrence

494   frequencies of 18.1 % and 17.4 %, respectively, while the liquid clouds had the least occurrence

495   frequency of 10.1 %. The percentages of non-drizzling, virga and drizzling for mixed-phase

496   clouds were 50 %, 21 %, and 29 %, and the drizzling frequencies of mixed-phase clouds

497   strongly depend on H_{top}, that is, higher drizzling frequencies occurred mostly at higher H_{top}.

498   4.   The meridional distributions of H_{base}, H_{top} and ΔH are nearly independent on

499   latitude. However, their corresponding temperatures increased about 8 K from 69 °S to 43 °S.

500   The meridional variation of LWPs mimics that of cloud temperatures, having an increasing

501   trend from south to north. The mean PWV increased dramatically from ~ 5 mm at 69 °S to ~18

502   mm at 43 °S due to increased sea surface and atmospheric temperatures. More liquid clouds

503   occurred over NSO but very few occurred over SSO, whereas more mixed-phase clouds

504   occurred over SSO than over NSO. There were no significant differences in ice clouds

505   occurrences between NSO and SSO.

506   5.   The nearly same median values of reflectivity, Doppler velocity and spectrum

507   width in both liquid and mixed-phase clouds over NSO suggest that the ice particle sizes in

508   mixed-phase clouds are comparable to cloud droplets and drizzle drops. The uniform vertical

509   distributions of Doppler velocity and spectrum width suggest well-mixed liquid cloud droplets

510   and ice particles throughout the cloud layer in the mixed-phase clouds over NSO, which are

511   quite different from those over the DOE ARM NSA site where the liquid topped mixed-phase

512   low-level clouds are common. The median values of reflectivity and Doppler spectrum width

513   over SSO were lower and narrower than those over NSO, indicating lack of large ice particles

514   in the polar region.

515   These results provide comprehensive statistical properties of all clouds over the SO during

516   MARCUS, including the occurrence frequencies of different types of clouds and their

517   corresponding cloud macrophysical properties. We also examined the meridional and vertical

518   distributions of the classified cloud properties. These statistics can be used as ground truth to

519   evaluate satellite retrieved cloud properties and model simulations over the SO. The results of this

520   study will help to advance our understanding of these clouds, which may lead to improved model

521   simulations over the SO as well as a better representation of global climate.

522

523   *Data availability.* Data used in this study can be accessed from the DOE ARM's Data Discovery at

524   https://adc.arm.gov/discovery/

525

Atmospheric
Measurement
Techniques
Discussions

526   *Author contributions.* The idea of this study is discussed by BX, XD, and XZ. BX and XZ performed

527   the analyses and BX wrote the manuscript. BX, XD, XZ and PW participated in scientific discussions

528   and provided substantial comments and edits on the paper.

529

530   *Competing interests.* The authors declare that they have no conflict of interest.

531

540

541

542

543   **References.**

544   Albrecht, B. A.: Aerosols, cloud microphysics, and fractional cloudiness, Science,

545   doi:10.1126/science.245.4923.1227, 1989.

546   Bodas-Salcedo, A., Mulcahy, J. P., Andrews, T., Williams, K. D., Ringer, M. A., Field, P. R. and

547   Elsaesser, G. S.: Strong Dependence of Atmospheric Feedbacks on Mixed-Phase

548   Microphysics and Aerosol-Cloud Interactions in HadGEM3, J. Adv. Model. Earth Syst.,

549   doi:10.1029/2019MS001688, 2019.

550   Bony, S., Stevens, B., Frierson, D. M. W., Jakob, C., Kageyama, M., Pincus, R., Shepherd, T. G.,

551   Sherwood, S. C., Siebesma, A. P., Sobel, A. H., Watanabe, M. and Webb, M. J.: Clouds,

552   circulation and climate sensitivity, Nat. Geosci., doi:10.1038/ngeo2398, 2015.

553   Chubb, T. H., Jensen, J. B., Siems, S. T. and Manton, M. J.: In situ observations of supercooled

554   liquid clouds over the Southern Ocean during the HIAPER Pole-to-Pole Observation

555   campaigns, Geophys. Res. Lett., doi:10.1002/grl.50986, 2013.

556   Dong, X., Xi, B., Kennedy, A., Minnis, P. and Wood, R.: A 19-month record of marine aerosol-

557   cloud-radiation properties derived from DOE ARM mobile facility deployment at the

558   Azores. Part I: Cloud fraction and single-layered MBL cloud properties, J. Clim.,

559   doi:10.1175/JCLI-D-13-00553.1, 2014.

560   Hu, Y., Rodier, S., Xu, K. M., Sun, W., Huang, J., Lin, B., Zhai, P. and Josset, D.: Occurrence,

561   liquid water content, and fraction of supercooled water clouds from combined

562   CALIOP/IIR/MODIS   measurements,   J.   Geophys.   Res.   Atmos.,

563   doi:10.1029/2009JD012384, 2010.

564   Intrieri, J. M., Fairall, C. W., Shupe, M. D., Persson, P. O. G., Andreas, E. L., Guest, P. S. and

565   Moritz, R. E.: An annual cycle of Arctic surface cloud forcing at SHEBA, J. Geophys. Res.

566   Ocean., doi:10.1029/2000jc000439, 2002.

567   Klein, S. A., Hall, A., Norris, J. R. and Pincus, R.: Low-Cloud Feedbacks from Cloud-Controlling

568   Factors: A Review, Surv. Geophys., doi:10.1007/s10712-017-9433-3, 2017.

569   Kalesse, H., de Boer, G., Solomon, A., Oue, M., Ahlgrimm, M., Zhang, D., Shupe, M. D., Luke,

570   E. and Protat, A.: Understanding rapid changes in phase partitioning between cloud liquid

571   and ice in stratiform mixed-phase clouds: An arctic case study, Mon. Weather Rev.,

572   doi:10.1175/MWR-D-16-0155.1, 2016.

Atmospheric
Measurement
Techniques
Discussions

573   Lang, F., Huang, Y., Siems, S. T. and Manton, M. J.: Characteristics of the Marine Atmospheric

574   Boundary Layer Over the Southern Ocean in Response to the Synoptic Forcing, J. Geophys.

575   Res. Atmos., doi:10.1029/2018JD028700, 2018.

576   Listowski, C., Delanoë, J., Kirchgaessner, A., Lachlan-Cope, T. and King, J.: Antarctic clouds,

577   supercooled liquid water and mixed phase, investigated with DARDAR: Geographical and

578   seasonal variations, Atmos. Chem. Phys., doi:10.5194/acp-19-6771-2019, 2019.

579   Mace, G. G., Zhang, Q., Vaughan, M., Marchand, R., Stephens, G., Trepte, C. and Winker, D.: A

580   description of hydrometeor layer occurrence statistics derived from the first year of merged

581   Cloudsat and CALIPSO data, J. Geophys. Res. Atmos., doi:10.1029/2007JD009755, 2009.

582   Mace, G. G. J. and Protat, A.: Clouds over the Southern Ocean as observed from the R/V

583   investigator during CAPRICORN. Part I: Cloud occurrence and phase partitioning, J. Appl.

584   Meteorol. Climatol., doi:10.1175/JAMC-D-17-0194.1, 2018.

585   Mace, G. G., Protat, A., Humphries, R. S., Alexander, S. P., McRobert, I. M., Ward, J., Selleck,

586   P., Keywood, M. and McFarquhar, G. M.: Southern Ocean Cloud Properties Derived From

587   CAPRICORN and MARCUS Data, J. Geophys. Res. Atmos., doi:10.1029/2020JD033368,

588   2021.

589   Marchand, R., Ackerman, T., Westwater, E. R., Clough, S. A., Cady-Pereira, K. and Liljegren, J.

590   C.: An assessment of microwave absorption models and retrievals of cloud liquid water

591   using clear-sky data, J. Geophys. Res. Atmos., doi:10.1029/2003jd003843, 2003.

592   Marchand, R., Wood, R., Bretherton, C., McFarquhar, G., Protat, A., Quinn, P., Siems, S., Jakob,

593   C., Alexander, S., Weller, B.: The Southern Ocean Clouds, Radiation Aerosol Transport

594   Experimental   Study   (SOCRATES),   whitepaper   available   from

595   http://www.atmos.washington.edu/socrates/SOCRATES_white_paper_Final_Sep29_201

Atmospheric
Measurement
Techniques
Discussions

Open Access

EGU

596   4.pdf, 2014.

597   Mccoy, D. T., Hartmann, D. L. and Grosvenor, D. P.: Observed Southern Ocean cloud properties

598   and shortwave reflection. Part II: Phase changes and low cloud feedback, J. Clim.,

599   doi:10.1175/JCLI-D-14-00288.1, 2014.

600   McFarquhar, G., Bretherton, C., Alexander, S., DeMott, P., Marchand, R., Protat, A., Quinn, P.,

601   Siems, S., Weller, R., Wood, R.: Measurements of Aerosols, Radiation, and Clouds over

602   Sothern Ocean (MARCUS) Science Plan, DOE ARM Climate Research Facility.,

603   DOE/SC-ARM-16-011, available at: http://arm.gov/publications/programdocs/doe-sc-

604   arm-16-011.pdf, 2016.

605   Mohrmann, J., Finlon, J., Atlas, R., Lu, J., Hsiao, I., Wood, R.: University of Washington Ice-

606   Liquid Discriminator single particle phase classifications and 1 Hz particle size

607   distributions/heterogeneity estimate, Version 1.0. UCAR/NCAR - Earth Observing

608   Laboratory., doi:10.26023/PA5W-4DRX-W50A, Last Access: Nov 01, 2021

609   Morrison, H., De Boer, G., Feingold, G., Harrington, J., Shupe, M. D. and Sulia, K.: Resilience of

610   persistent Arctic mixed-phase clouds, Nat. Geosci., doi:10.1038/ngeo1332, 2012.

611   Qiu, S., Dong, X., Xi, B. and Li, J. L. F.: Characterizing Arctic mixed-phase cloud structure and

612   its relationship with humidity and temperature inversion using ARM NSA observations, J.

613   Geophys. Res., doi:10.1002/2014JD023022, 2015.

614   Sassen, K.: The polarization lidar technique for cloud research: a review and current assessment,

615   Bull. - Am. Meteorol. Soc., doi:10.1175/1520-0477(1991)072<1848:TPLTFC>2.0.CO;2,

616   1991.

617   Shupe, M. D., Uttal, T. and Matrosov, S. Y.: Arctic cloud microphysics retrievals from surface-

618   based remote sensors at SHEBA, J. Appl. Meteorol., doi:10.1175/JAM2297.1, 2005.

619   Shupe, M.: A ground-based multisensory cloud phase classifier, Geophys. Res. Lett.,
620   doi:10.1029/2007GL031008, 2007.

621   Stanfield, R. E., Dong, X., Xi, B., Kennedy, A., Del Genio, A. D., Minnis, P. and Jiang, J. H.:
622   Assessment of NASA GISS CMIP5 and Post-CMIP5 Simulated Clouds and TOA
623   Radiation Budgets Using Satellite Observations. Part I: Cloud Fraction and Properties, J.
624   Clim., doi:10.1175/jcli-d-13-00558.1, 2014.

625   Stanfield, R. E., Dong, X., Xi, B., Del Genio, A. D., Minnis, P., Doelling, D. and Loeb, N.:
626   Assessment of NASA GISS CMIP5 and post-CMIP5 simulated clouds and TOA radiation
627   budgets using satellite observations. Part II: TOA radiation budget and CREs, J. Clim.,
628   doi:10.1175/JCLI-D-14-00249.1, 2015.

629   Stocker, T. F., Qin, D., Plattner, G. K., Tignor, M. M. B., Allen, S. K., Boschung, J., Nauels, A.,
630   Xia, Y., Bex, V. and Midgley, P. M.: Climate change 2013 the physical science basis:
631   Working Group I contribution to the fifth assessment report of the intergovernmental panel
632   on climate change., 2013.

633   Wu, P., Dong, X. and Xi, B.: Marine boundary layer drizzle properties and their impact on cloud
634   property retrieval, Atmos. Meas. Tech., doi:10.5194/amt-8-3555-2015, 2015.

635   Wu, P., Dong, X., Xi, B., Liu, Y., Thieman, M. and Minnis, P.: Effects of environment forcing on
636   marine boundary layer cloud-drizzle processes, J. Geophys. Res.,
637   doi:10.1002/2016JD026326, 2017.

638   Wu, P., Dong, X. and Xi, B.: A climatology of marine boundary layer cloud and drizzle properties
639   derived from ground-based observations over the azores, J. Clim., doi:10.1175/JCLI-D-20-
640   0272.1, 2020.

641 Xi, B., Dong, X., Minnis, P. and Khaiyer, M. M.: A 10 year climatology of cloud fraction and

642   vertical distribution derived from both surface and GOES observations over the DOE ARM

643   SPG site, J. Geophys. Res. Atmos., doi:10.1029/2009JD012800, 2010.

644 Zelinka, M. D., Myers, T. A., McCoy, D. T., Po-Chedley, S., Caldwell, P. M., Ceppi, P., Klein, S.

645   A. and Taylor, K. E.: Causes of Higher Climate Sensitivity in CMIP6 Models, Geophys.

646   Res. Lett., doi:10.1029/2019GL085782, 2020.

647 Zhao, L., Zhao, C., Wang, Y., Wang, Y. and Yang, Y.: Evaluation of Cloud Microphysical

648   Properties Derived From MODIS and Himawari-8 Using In Situ Aircraft Measurements

649   Over the Southern Ocean, Earth Sp. Sci., doi:10.1029/2020EA001137, 2020.

Table 1. Minimum cloud base heights (H_{base}), maximum cloud top heights (H_{top}), and liquid water paths (LWPs) (all samples, single-layered, multilayered) of all seven types of clouds over the Southern Ocean. Cloud heights have unit of kilometer, and LWP has unit of g m^{-2}.

	LOW	MID	MOL	HGH	HOM	HML	HOL
H_{base} ± std	0.92 ± 0.57	4.14 ± 0.61	1.37 ± 0.96	8.51 ± 2.23	4.70 ± 0.80	1.22 ± 0.98	1.14 ± 1.12
min, max	0.06, 2.86	3.00, 5.84	0.06, 5.27	6.00, 18.67	3.01, 7.72	0.06, 7.81	0.07, 10.37
H_{top} ± std	1.62 ± 0.63	4.88 ± 0.68	4.29 ± 0.89	9.75 ± 2.13	7.93 ± 1.27	7.81 ± 1.35	8.93 ± 1.66
min, max	0.29, 3.0	3.17, 6.0	1.39, 5.99	6.20,18.79	5.47, 17.98	3.62,17.38	1.79, 17.56
LWP ± std	122.4±134.2	86.7±124.5	168.7±236.7	/	40.9±40.8	169.2±238.4	129.8±202.
Max LWP	1470.8	501.1	1937.1	/	345.7	1819.3	1785.2
LWP ± std (single layer)	126.6±138.1	88.7±128.9	193.1±271.9	/	48.7±51.7	270.8±349.5	/
max	1470.8	501.1	1937.1	/	345.7	1819.3	/
LWP ± std (multi-layer)	96.2±103.4	77.2±109.2	139.0±180.7	/	32.3±21.3	148.4±202.4	129.8±202.
max	842.3	305.6	1830.2	/	86.8	1690.7	1785.2
Multi-layer percentage %	18.1	39.6	50.0	44.9	73.1	77.7	100

* The definition of the cloud types as follow: LOW (H_{base} and $H_{top} \leq 3\ km$); MID ($H_{base} > 3\ km$ and $H_{top} \leq 6\ km$); HGH ($H_{base} > 6\ km$); MOL ($H_{base} < 3\ km$ and $H_{top} \leq 6\ km$); HOM ($3\ km < H_{base} < 6\ km$ and $H_{top} > 6\ km$); HML ($H_{base} < 3\ km$, $H_{top} \geq 6\ km$ with a MID layer); HOL (LOW and HGH appear at the same time).

Table 2a. Comparison of cloud phase identifications between our classification method and Shupe et al. (2005) method in each 5-min measurements, the unit is number of 5-min samples.

Shupe / this study	Liquid (this study)	Mixed-phase (this study	Ice (this study)
Liquid	468	490	0
Mixed-phase	98	3840	0
Ice	81	0	1195

*Numbers denote the cloud sample classifications between two methods. For example, the number 98 denote a total of 98 samples are classified as Mixed-phase using Shupe's method, while are classified as Liquid using this study's method.

Table 2b. The cloud phase partitioning from CDP and 2DS during SOCRATES. Cloud Droplet Probe (CDP) measures particle size from 2 to 50 um in diameter; Two-Dimensional Stereo Probe (2DS) measures particle size from 50 to 5000 um in diameter.

Phase partitioning	1 second	10 seconds	30 seconds
Samples #	27280	2255	836
Liquid, %	58.8	26.2	18.8
Mixed-phase, %	38.9	69.1	77.0
Ice, %	2.3	4.7	4.2

Table 3. Liquid, mixed, ice and OTHER phases of cloud properties within the single-layered low-level clouds

Phase	Samples	H_{base}, km	H_{top}, km	ΔH, km	LWP, g m^{-2}	PWV, mm
Liquid	697	0.424±0.204	1.327±0.242	0.903	113.6±90.1	15.7±3.5
Mixed	3777	0.834±0.465	1.434±0.617	0.587	119.7±136.6	8.9±5.0
Ice	1205	1.218±0.635	1.737±0.651	0.519	0	8.4±4.5
OTHER	1255	0.700±0.454	1.774±0.571	1.074	141.9±137.5	11.4±5.9
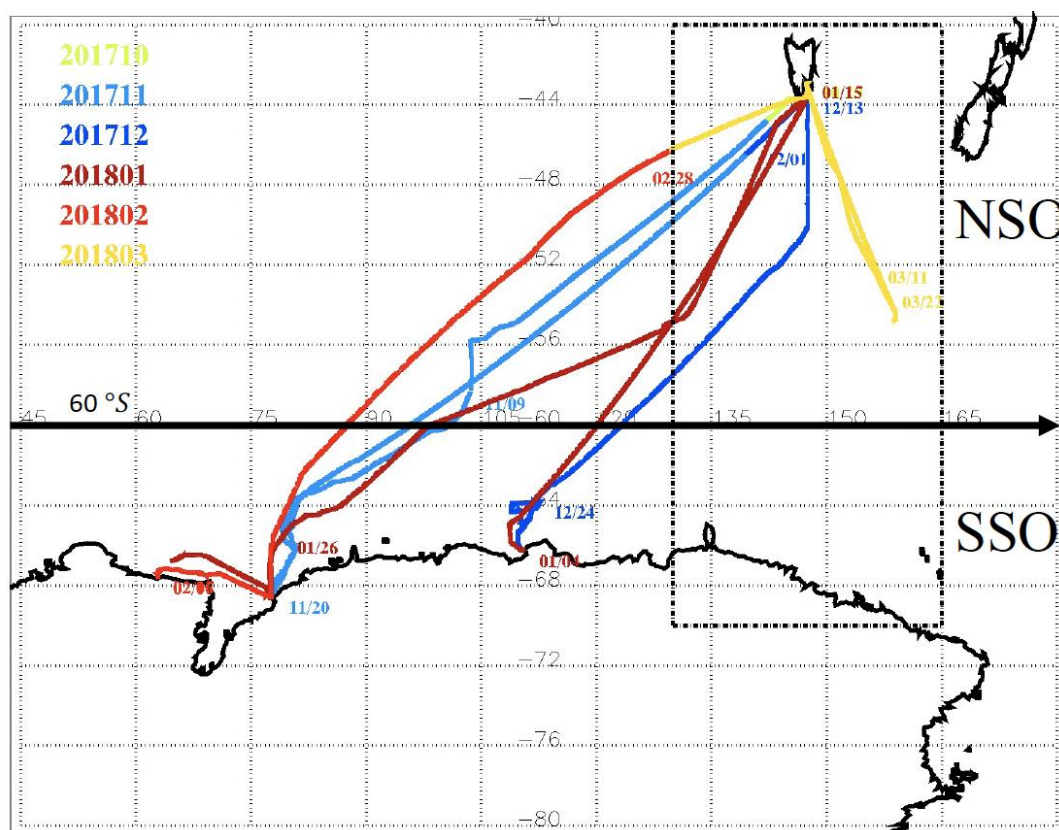
Figure 1. Shiptrack measurements between Hobart, Australia and Antarctica. Different colors represent different month's shiptracks from Oct. 29, 2017 to Mar. 23, 2018 during MARCUS. Along the shiptracks, the study domain is separated into northern (NSO) and southern (SSO) parts of the Southern Ocean with a demarcation line of 60 °S in order to study the clouds over the mid-latitudes (North of 60 °S) and Polar region (South of 60 °S). The black dotted rectangle represents the SOCRATES study domain. Some of the dates have labeled along the shiptracks, which can indicate the direction of the ship traveled.
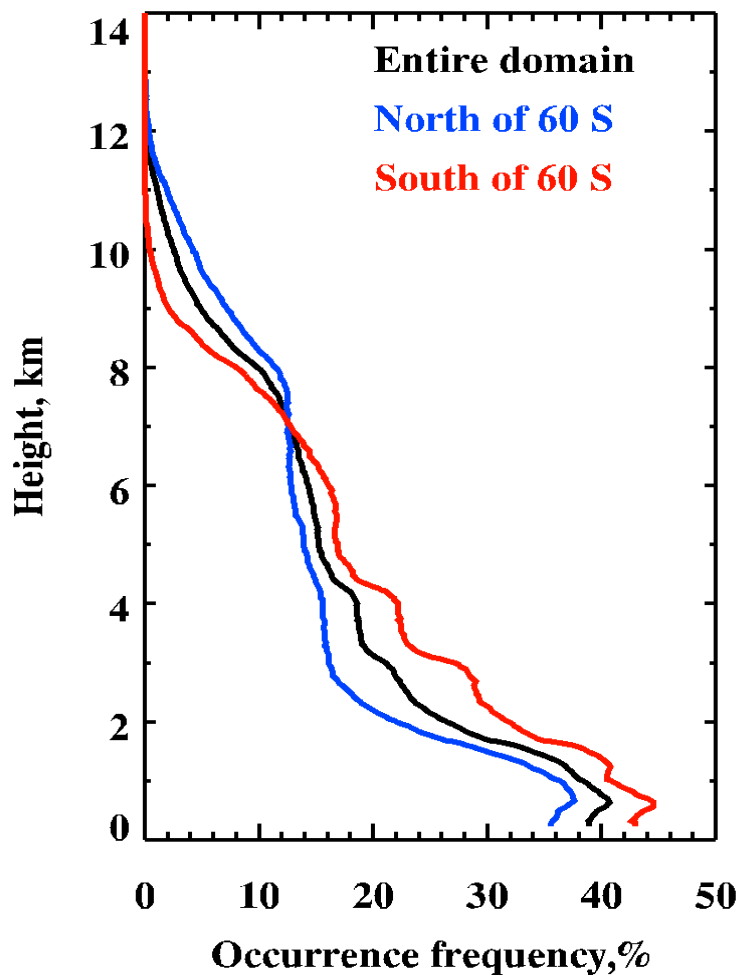
Figure 2. Mean vertical distributions of total clouds derived from ARM radar-lidar observations with a 5-min temporal resolution and a 30-m vertical resolution during MARCUS.
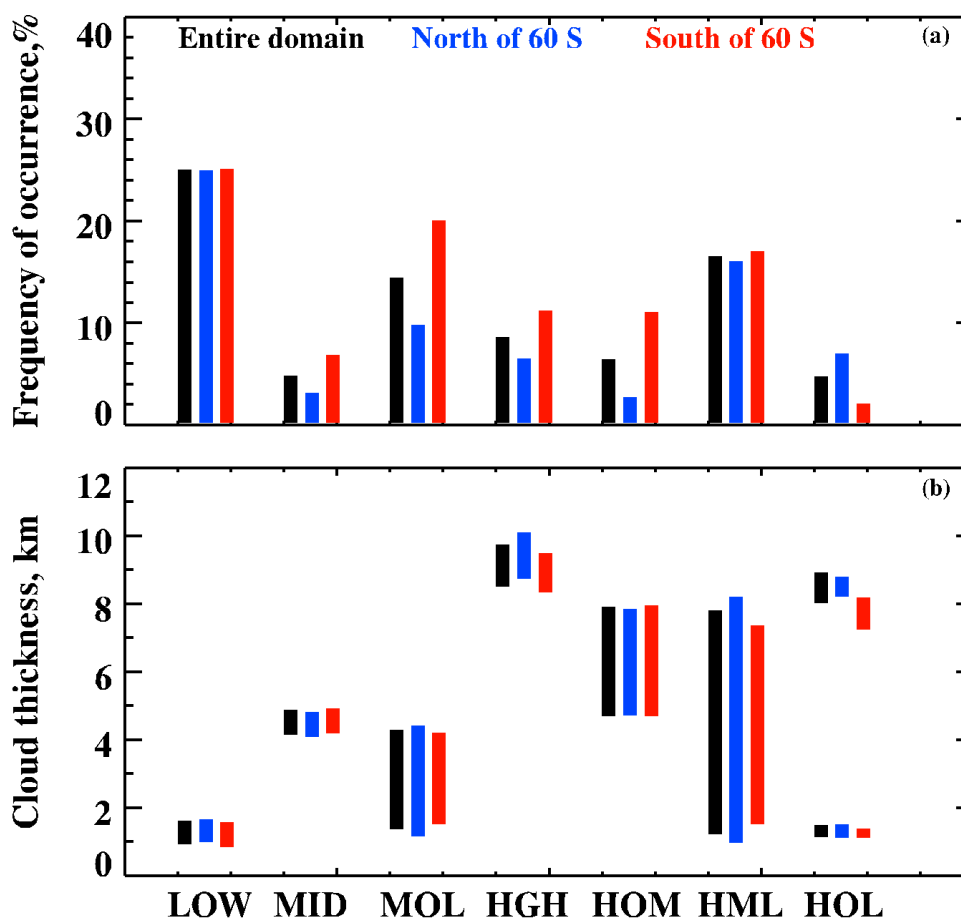
Figure 3. (a) Occurrence frequencies of categorized clouds by their vertical structures. LOW, single‑layered low clouds (H_{base} and $H_{top} \leq 3\ km$); MID, single-layered middle clouds ($H_{base} > 3\ km$ and $H_{top} \leq 6\ km$); MOL, MID over LOW ($H_{base} < 3\ km$ and $H_{top} \leq 6\ km$); HGH, single-layered high clouds ($H_{base} > 6\ km$); HOM, HGH over MID ($3\ km < H_{base} < 6\ km$ and $H_{top} > 6\ km$); HML, HGH over MID and LOW ($H_{base} < 3\ km$, $H_{top} \geq 6\ km$ with a MID layer); and HOL, HGH over LOW (LOW and HGH appear at the same time). (b) Cloud thickness for each type of clouds (bar), the top and bottom of the bar represent the maximum cloud-top and minimum cloud-base heights, respectively. Black, blue, and red bars represent the entire domain (Lat:41-69 °S; Long: 60-160° E), north of 60 °S (NSO), and south of 60°S (SSO), respectively, during the MARCUS field campaign (10/2017-3/2018).
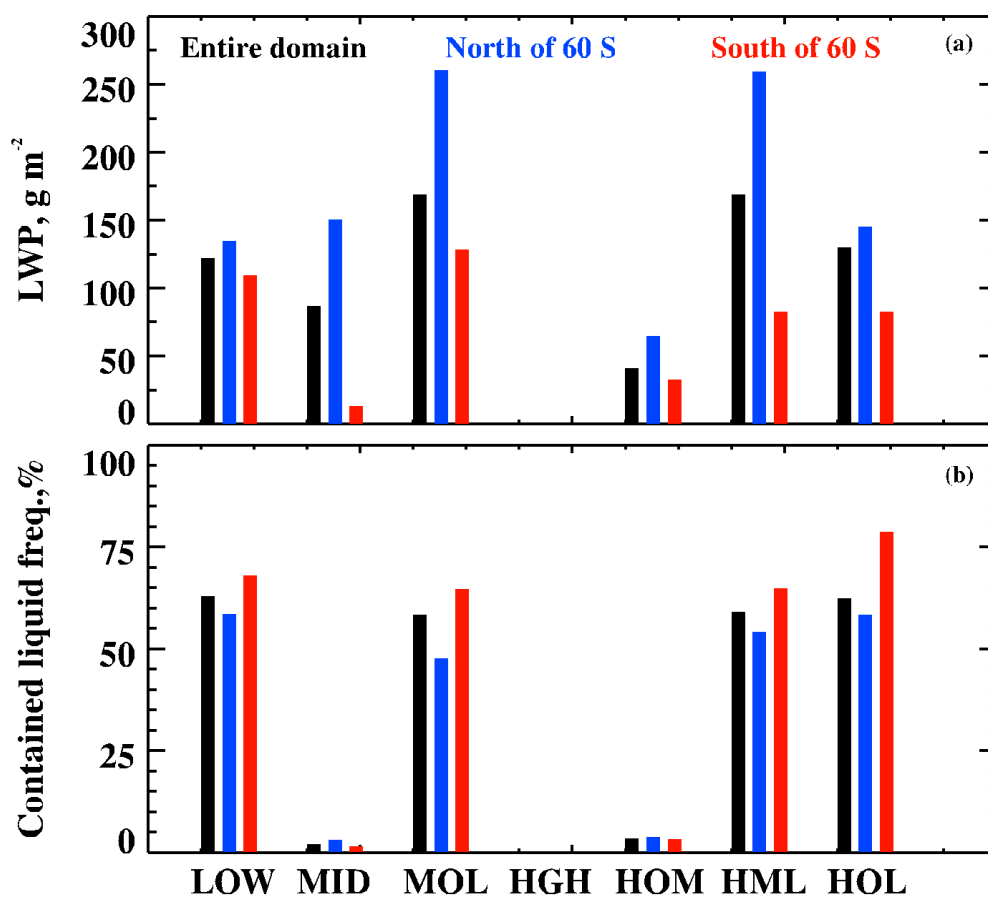
Figure 4. (a) Cloud liquid water paths (*LWP*s) retrieved from microwave radiometer (MWR) measured brightness temperature using a physical retrieval method for each type of cloud. (b) The occurrence frequencies of LWPs> 10 gm^{-2} for each type of clouds

Atmospheric
Measurement
Techniques
Discussions

Open Access

EGU

Phase classification algorithm for single layered low level clouds
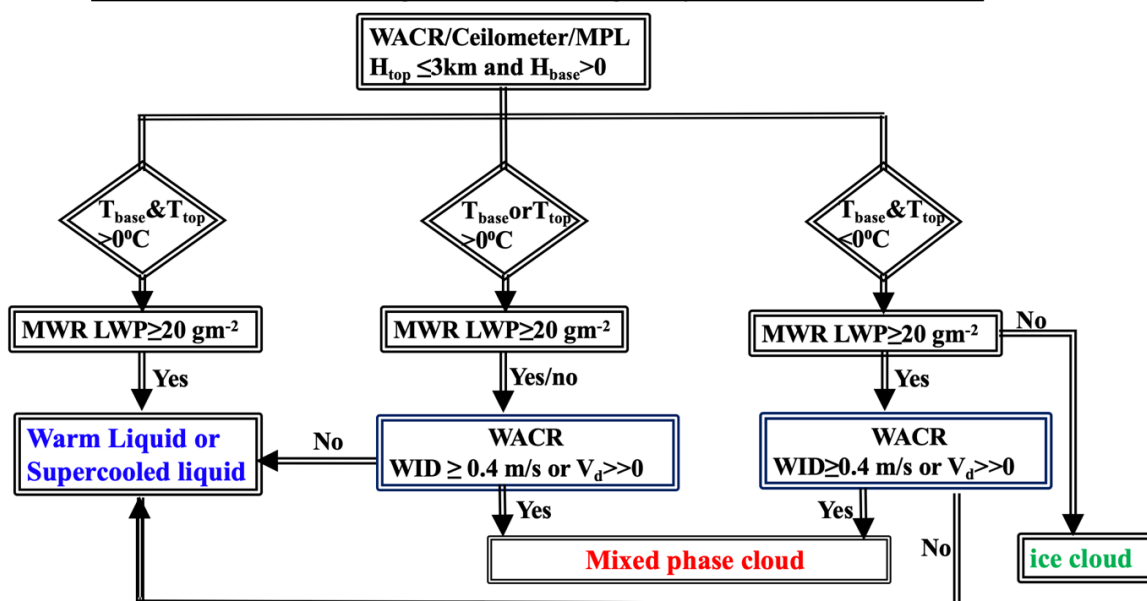
Figure 5. A flow chart for phase classification of single-layered low-level clouds. W-Band (95 GHz) ARM Cloud Radar (WACR) provides radar spectrum width (*WID*) and Doppler velocity (V_d).
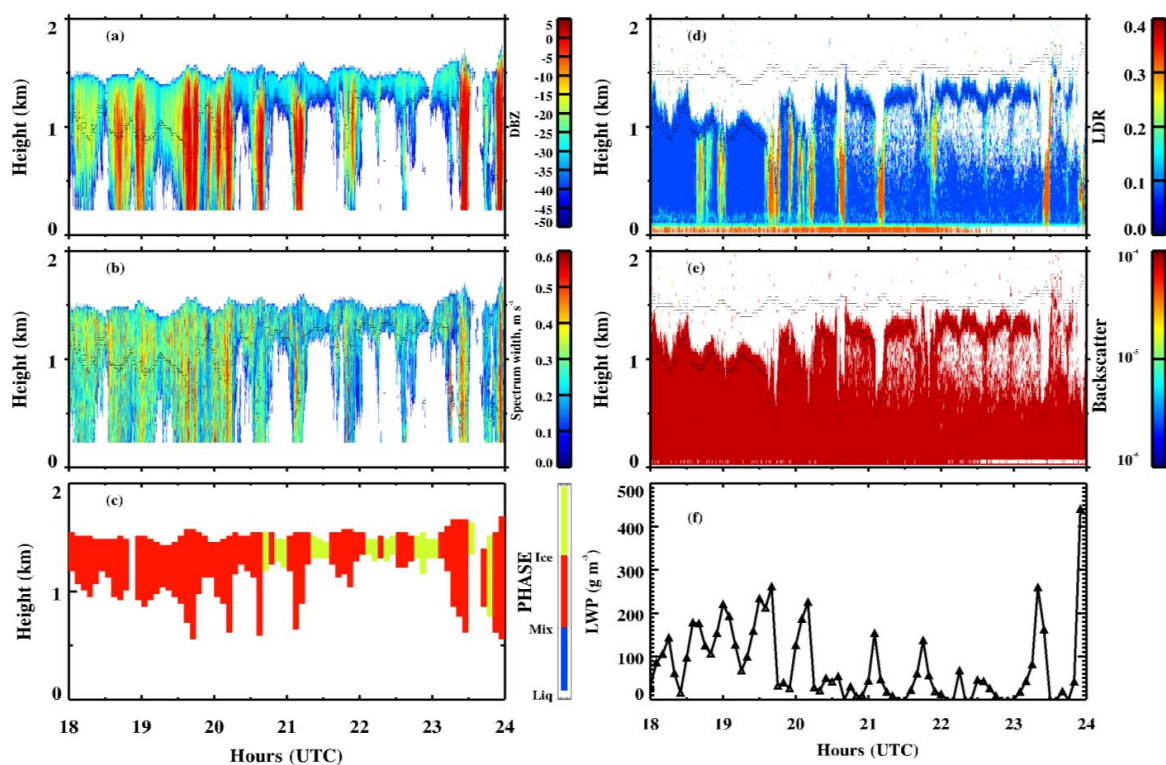
Figure 6. A case study that shows our phase classification (left column) and Micropulse Lidar linear depolarization ratios (*LDR*) and backscatter. W-Band (95 GHz) ARM Cloud Radar (WACR) reflectivity shows in (a) and spectrum width shows in (b); The phase classification shows in (c); MPL *LDR* shows in (d) and backscatter shows in (e); and *LWP* shows in (f).
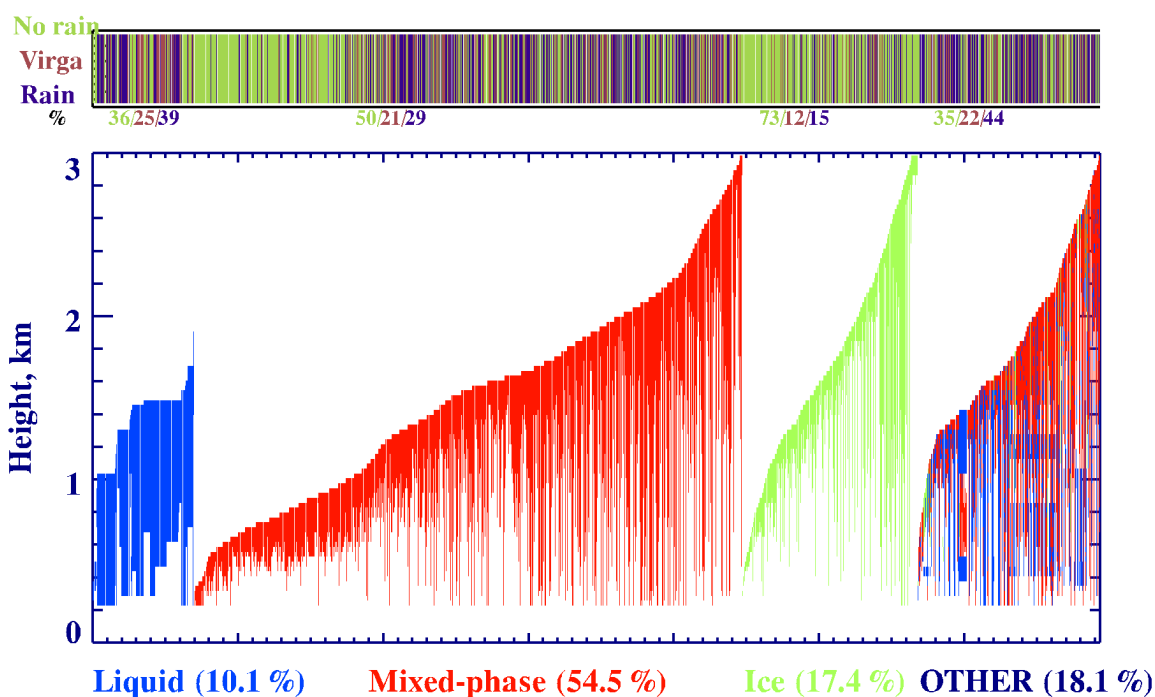
Figure 7. (Upper Panel) The drizzling status for each categorized cloud type, e.g., no rain (yellow-green), virga (brown) and rain (navy blue), the percentages shown below the x-axis represent the portion of drizzling in each type of clouds; And (Bottom Panel) the percentages and vertical distributions of classified liquid, mixed-phase, ice, and 'OTHER' clouds for each column in the single-layered low-level clouds, represented by different colors, over the entire domain during MARCUS. Each line represents one 5-min sample.
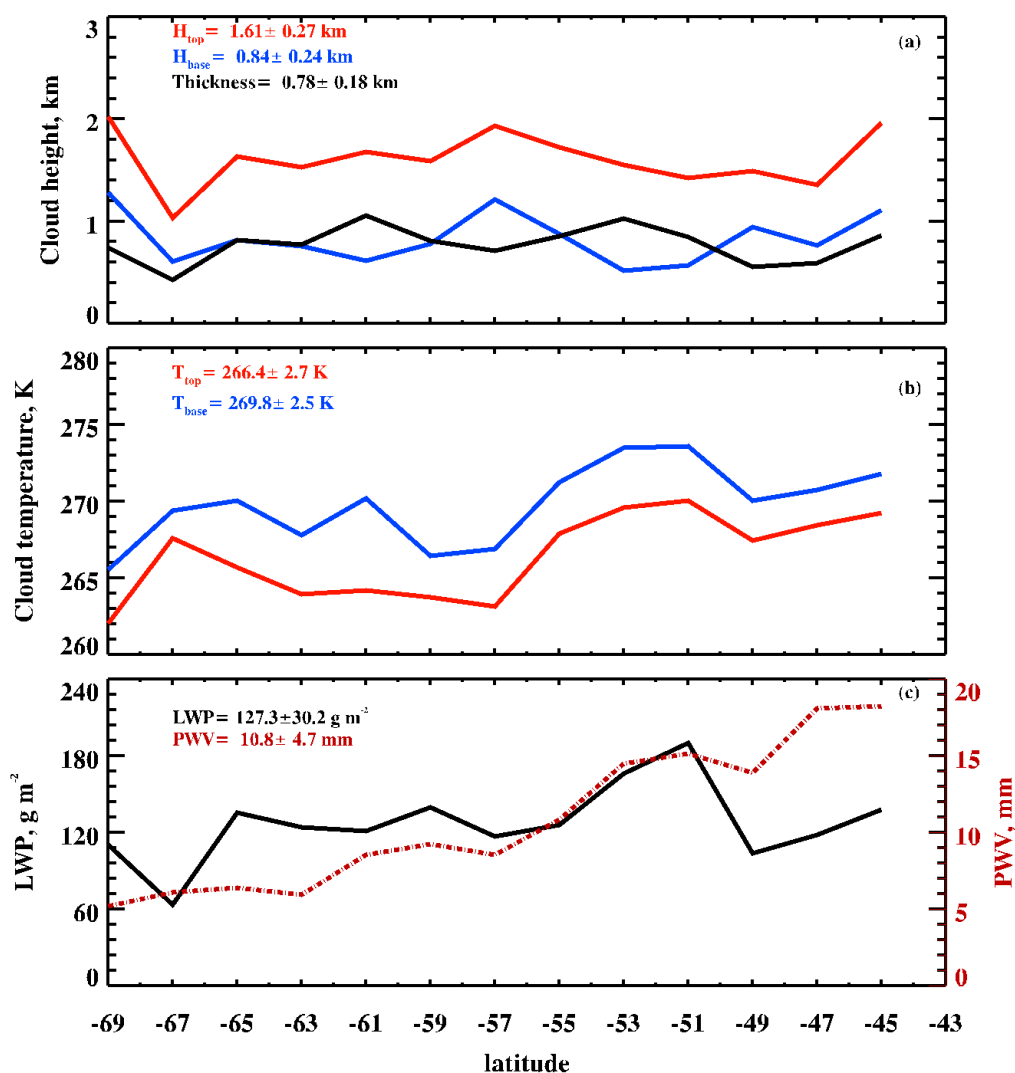
Figure 8. Meridional variations of single-layered low-level cloud properties: (a) cloud-base (H_{base}) and -top (H_{top}) heights, and cloud thickness (ΔH), (b) cloud-base (T_{base}) and -top (T_{top}) temperatures, and (c) cloud liquid water path (*LWP*) and precipitable water vapor (PWV) over the entire domain during MARCUS.
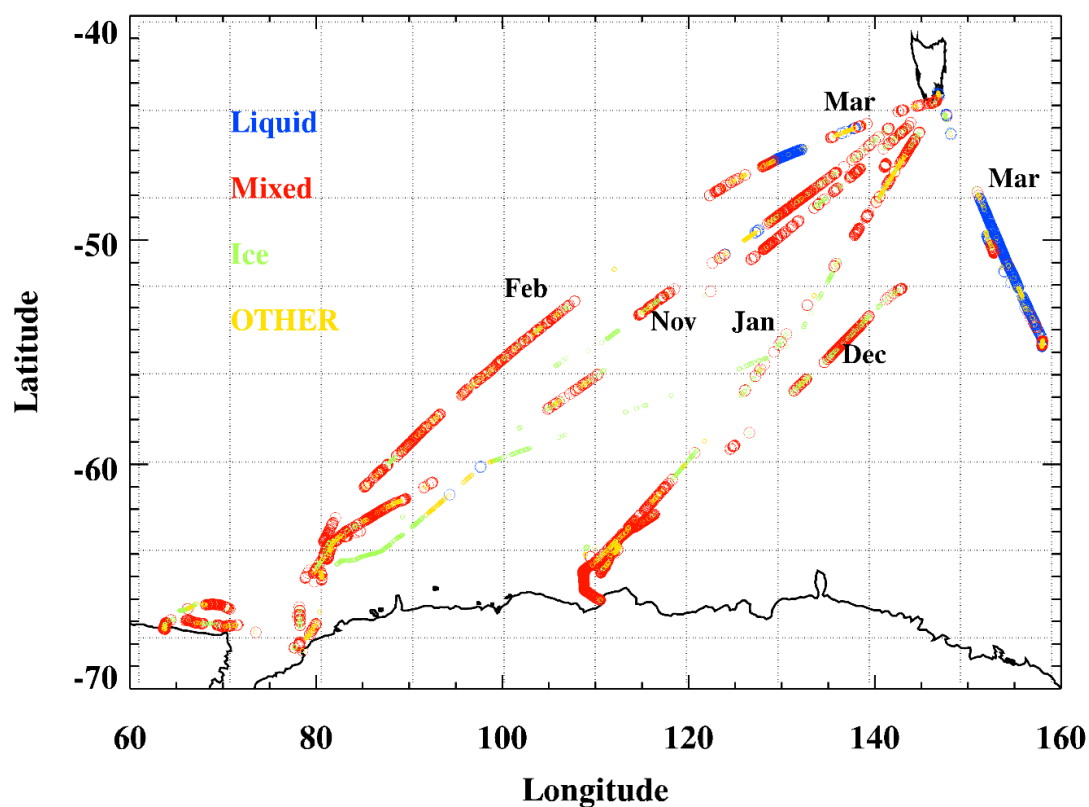
Figure 9. The latitudinal and longitudinal distributions of classified mixed-phase, liquid, and ice clouds in the single-layered low-level clouds. The liquid (blue), mixed (red), ice (light green), and OTHER (yellow) are shown along each shiptrack from October 2017 to March 2018 during MARCUS.
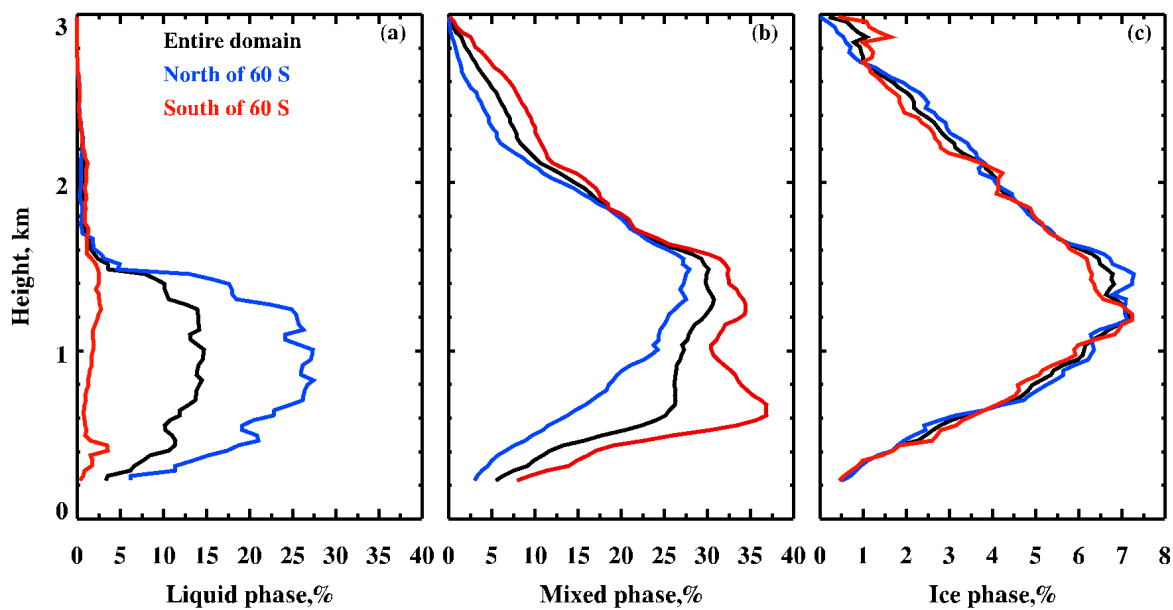
Figure 10. Occurrence frequencies of classified mixed-phase, liquid, and ice clouds over the entire domain (black), North of 60 °S (blue) and South of 60 °S during MARCUS.
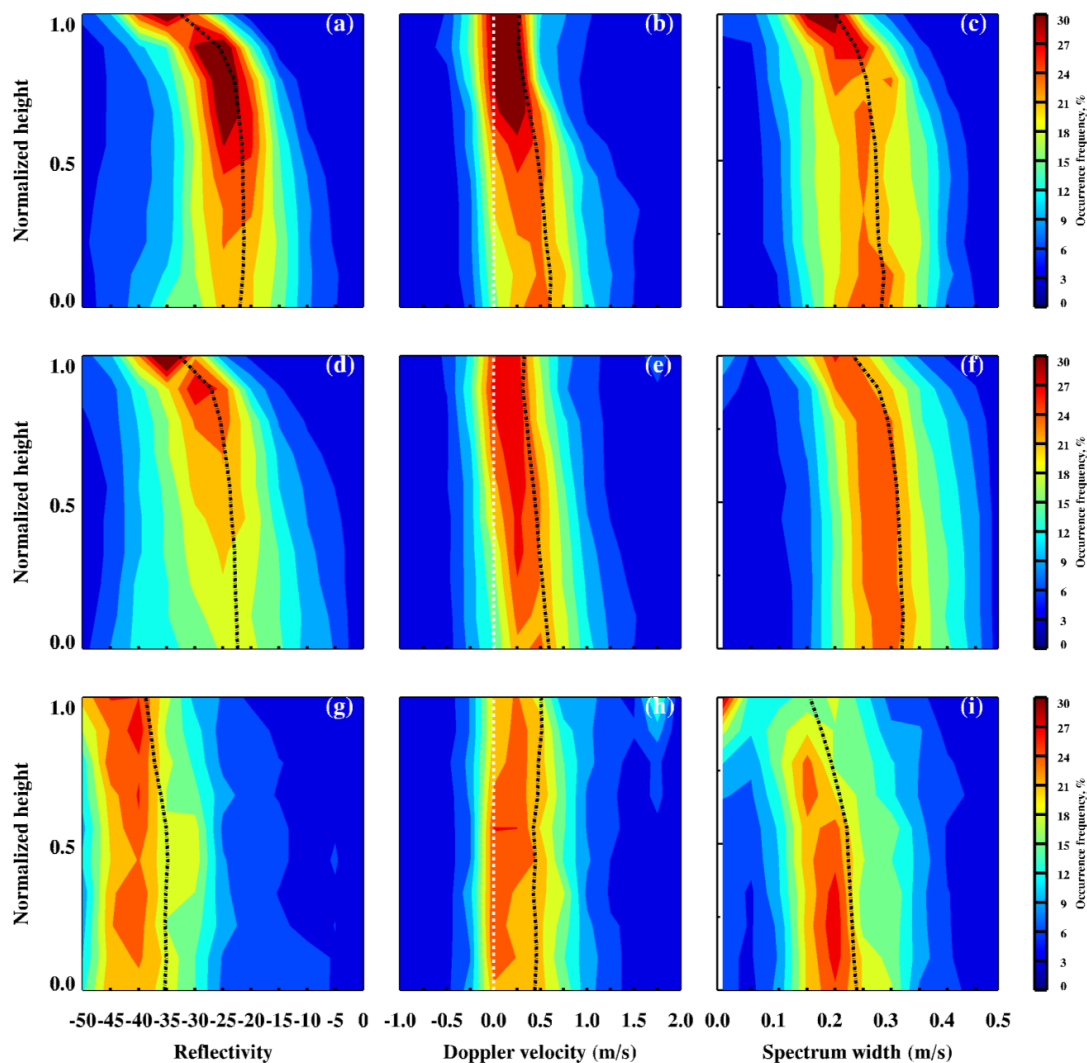
Figure 11. Normalized vertical distributions of a) radar reflectivity, b) Doppler velocity and c) spectrum width for the classified liquid (upper panel), mixed-phase (d to f, middle panel) and ice (g to i, bottom panel) clouds over the North of 60 °S during MARCUS IOP. Normalized height is defined as $= \frac{H - H_{base}}{H_{top} - H_{base}}$ where cloud base is denoted as 0 and cloud top is 1. The black lines represent the median values and the white lines in Doppler velocity represent the reference of 0.0 m s^{-1}.
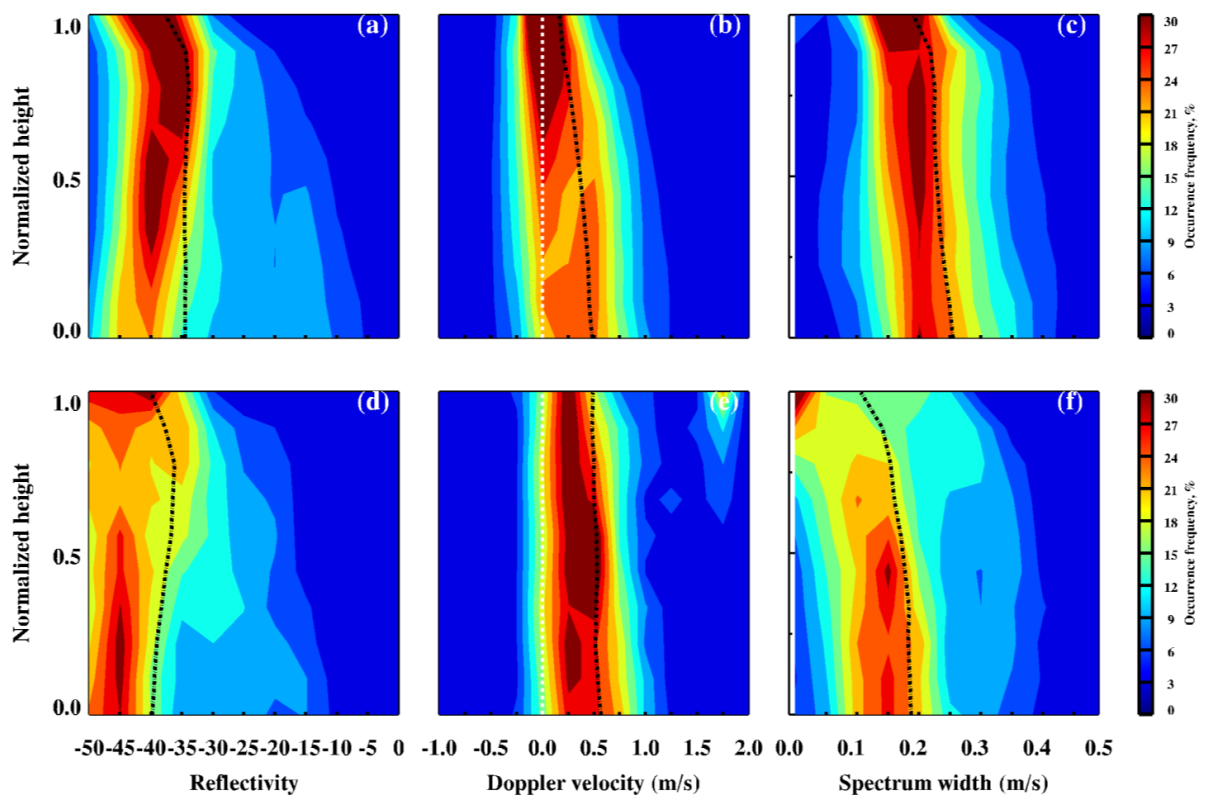
Figure 12. Same as Fig. 11 but only for mixed-phase (a to c, upper panel) and ice (d to f, bottom panel) over the south of 60 °S during MARCUS.